Detection of acoustic events in lavender for measuring xylem vulnerability to embolism and cellular damage

Lia Lamacque, Florian Sabin, Thierry Améglio, Stéphane Herbette, Guillaume Charrier

RESEARCH PAPER

Detection of acoustic events in lavender for measuring xylem vulnerability to embolism and cellular damage

Lia Lamacque[1,2,*], Florian Sabin[1], Thierry Améglio[1], Stéphane Herbette[1], and Guillaume Charrier[1,†]

[1] Université Clermont Auvergne, INRAE, PIAF, F-63000 Clermont-Ferrand, France

[2] Institut Technique Interprofessionnel Plantes à Parfum, Médicinal, Aromatiques et Industrielles, 26740 Montboucher-sur-Jabron, France

* Present address: INRAE, Plant Pathology, Montfavet, F-84140, France
† Correspondence: guillaume.charrier@inrae.fr

Abstract

Acoustic emission analysis is promising to investigate the physiological events leading to drought-induced injury and mortality. However, their nature and source are not fully understood, making this technique difficult to use as a direct measure of the loss of xylem hydraulic conductance. Acoustic emissions were recorded during severe dehydration in lavender plants (*Lavandula angustifolia*) and compared with the dynamics of embolism development and cell damage. The timing and characteristics of acoustic signals from two independent recording systems were compared by principal component analysis (PCA). Changes in water potential, branch diameter, loss of hydraulic conductance, and cellular damage were also measured to quantify drought-induced damages. Two distinct phases of acoustic emissions were observed during dehydration: the first one associated with a rapid loss of diameter and a significant increase in loss of xylem conductance (90%), and the second with slower changes in diameter and a significant increase in cellular damage. Based on PCA, a developed algorithm discriminated hydraulic-related acoustic signals from other sources, proposing a reconstruction of hydraulic vulnerability curves. Cellular damage preceded by hydraulic failure seems to lead to a lack of recovery. The second acoustic phase would allow detection of plant mortality.

Keywords: Acoustics, cavitation, cellular damages, dendrometer, hydraulic failure, lavender, plant mortality, xylem.

Introduction

Drought stress in plants leads to a cascade of physiological events as water content progressively decreases. Under mild stress, stomata close, thus limiting water losses through decreased transpiration. However, bulk water content continuously decreases via cuticular transpiration and leaky stomata (Martin-StPaul *et al.*, 2017). Under extreme drought conditions, the critical branch diameter at which the plant loses its ability to rehydrate is an indicator of plant mortality (~20% of branch diameter loss in lavender; Lamacque *et al.*, 2020). Plant mortality is observed after complete xylem hydraulic failure, when cellular damage increases dramatically (~5% of branch cellular damage; Lamacque *et al.*, 2020).

In the hydraulic system, water flows under a metastable state, according to the gradient in water potential (Dixon and Joly, 1895). When water losses (evapotranspiration) exceed water supply (root water uptake) and intrinsic pools

(capacitance), the tension in the xylem sap increases. Above a critical value, xylem sap metastability is disrupted, resulting in a sudden formation of gas bubbles (i.e. cavitation) that expand and embolize the xylem conducting elements (Lewis, 1988). Xylem embolism therefore decreases the sap flow, thereby inducing the dehydration of distal organs (e.g. leaves and buds; Tyree and Sperry, 1989). Xylem embolism is thus tightly correlated to plant mortality (Brodribb and Cochard, 2009; Barigah *et al.*, 2013; Anderegg *et al.*, 2016). Although the water potential inducing a loss of hydraulic conductivity >88% has long been considered as the plant mortality threshold in angiosperms under drought stress (Barigah *et al.*, 2013; Urli *et al.*, 2013; Li *et al.*, 2016), recent studies highlighted large variations in this critical level across and within species and thus the need to further investigate the mechanisms of drought-induced mortality (Nardini *et al.*, 2013; Hammond *et al.*, 2019; Mantova *et al.*, 2021).

Plant mortality is indirectly assessed through the inability to regrow or resprout once the stress is released. It is usually monitored until the following growing season to assess the actual death of the plant. The viability of living cells, including meristems, is thus key to predict plant survival (Guadagno *et al.*, 2017). However, hydraulic failure and cell viability have rarely been studied together (Charra-Vaskou *et al.*, 2012; Ganthaler and Mayr, 2015) although their interaction is probably key to predict drought mortality mechanisms (Lamacque *et al.*, 2020; Charrier *et al.*, 2021a). The distinction between these two processes is an important point to explore, in order to refine the detection of mortality.

Numerous methods have been used to quantify hydraulic failure, such as the gravimetric method (Sperry *et al.*, 1988) or the pressure sleeve (Ennajeh *et al.*, 2011). However, these methods are destructive and may produce unrealistic values by the induction of bubbles at sample ends whenever the tension of the sap is not released by successive cuttings (Wheeler *et al.*, 2013). X-ray microtomography allows spatialized observation of embolized xylem on a cross-section (Cochard *et al.*, 2015; Choat *et al.*, 2016; Nolf *et al.*, 2017). However, the exposure to high energy radiation has deleterious consequences on cellular viability (Petruzzellis *et al.*, 2018). Non-invasive methods have been developed more recently to measure the changes in light transmission caused by air spreading within xylem tissue of leaves and stems (Brodribb et al., 2016, 2017).

Cellular damage can be assessed through the amount of electrolytes released in solution or by staining techniques to detect living cells and therefore dead cells. This technique has been used to study the effect of various stress factors such as chilling (Herbette *et al.*, 2005; Mai *et al.*, 2009), frost (Charrier and Améglio, 2011; Guàrdia *et al.*, 2016), or drought stress (Guadagno *et al.*, 2017; Lamacque *et al.*, 2020).

The measurement of branch diameter variation allows continuous and non-invasive monitoring of the water status and growth of trees (Zweifel et al., 2001, 2006; Daudet *et al.*, 2004). The changes in branch diameter follow a daily and seasonal pattern as a result of several factors: irreversible radial growth, reversible living cell dehydration and rehydration, expansion of conducting elements due to the increase and relaxation of internal tensions, and thermal expansion and contraction (Daudet *et al.*, 2004; Zweifel *et al.*, 2005). Monitoring branch diameter changes is an accurate indicator of the ability to recover, in particular after a drought period (Lamacque *et al.*, 2020). The loss in diameter is a quantitative assessment of damage (i.e. injuries caused by a severe stress) and has been used to study the effect of frost (Améglio *et al.*, 2003; Charra-Vaskou *et al.*, 2016) or drought stress (Lamacque *et al.*, 2020). These types of damage result in a loss of ability to recover in relation to loss of conductance and cellular damage (Lamacque *et al.*, 2020). The amount of damage can be approximated by the ratio of initial diameter to recovered diameter after stress has been released (Lamacque *et al.*, 2020).

The detection of acoustic events has been used as a non-invasive technique to analyze a plant's response to drought (Milburn and Johnson, 1966; Tyree and Dixon, 1983). Acoustic events have been recorded under drought and frost stress, on potted and naturally growing plants (Lo Gullo and Salleo, 1992; Rosner *et al.*, 2006; Vergeynst *et al.*, 2014; Charrier *et al.*, 2017). The nucleation of bubbles in the xylem elements, observed by microscopic observations, generates acoustic events (Ponomarenko *et al.*, 2014). However, the cumulated number of acoustic events usually exceeds the theoretical number of xylem conducting elements in the sample (Rosner *et al.*, 2006; Kasuga *et al.*, 2015; Vergeynst *et al.*, 2015). Furthermore, acoustic events are also recorded after xylem conduits are fully embolized potentially as a result of cavitation events in fiber cells (Wolkerstorfer *et al.*, 2012; Nolf *et al.*, 2015). The cumulative rate of acoustic events is therefore not always proportional to the loss of hydraulic conductivity as cavitation events in non-conductive cells do not have any influence on xylem hydraulic conductance (e.g. fibers; Nolf *et al.*, 2015). The use of this technique has thus been limited, as a complete overview of acoustic sources is not clearly identified (Wolkerstorfer *et al.*, 2012; Kasuga *et al.*, 2015).

Distinguishing acoustic events associated with embolism formation in the conductive xylem conduits from those associated with events occurring in non-conductive cells would be a tremendous advance in interpreting results obtained from the non-invasive acoustic method. Taking acoustic event characteristics into account, such as amplitude, energy, and frequency, seems be a promising avenue for this purpose. Energy-weighted acoustic events seem more relevant from a hydraulic point of view (Mayr and Rosner, 2011; Kasuga *et al.*, 2015). During the freezing of walnut stems, Kasuga *et al.* (2015) identified that two types of acoustic events were generated, by frost-induced embolism and by intracellular freezing. Seasonal changes in the response to freezing temperature has been related to the process of cold acclimation of living cells (Charrier et al., 2014a, b). In dehydrating branches from grapevine, three clusters of events have been characterized:

high-, middle-, and low-frequency events (Vergeynst *et al.*, 2016). High-frequency signals were assumed to be generated by capillary action of water and fast contraction of the bark, while low-frequency signals were generated by microfractures (Vergeynst *et al.*, 2016). Mid-frequency signals seem to be linked to hydraulic failure and are probably generated by cavitation events.

Drought-induced mortality in lavender was associated with high levels of cellular damage rather than high levels of embolism in the branch (Lamacque *et al.*, 2020). We therefore expect that the development of embolism would stop earlier than cellular damage during an extreme drought. Based on the evidence that acoustic emissions (AEs) can be generated by cavitation events, cellular damage, and tissue fractures, we hypothesize that analyzing acoustic events based on the time of occurrence would help to identify their source. Earlier recorded acoustic events would be related to loss of hydraulic conductance, whereas later events would be linked to cellular damage and/or fiber discharge. Multivariate signal analysis would allow discrimination of AEs in relation to hydraulic failure and cellular damage. During an extreme dry-down, AEs were continuously monitored and stem diameter was measured and related to relevant physiological parameters: water potential, cellular damage, and loss of hydraulic conductivity. Based on intrinsic acoustic characteristics recorded, the multivariate signal analysis of acoustic events allowed discrimination of acoustic events from hydraulic and non-hydraulic origin and thus reproduced the dynamics of both the loss of hydraulic conductance and the cellular damage during a severe dehydration.

Materials and methods

Plant material

Experiments were carried out on a clonal variety of lavender (*Lavandula angustifolia* Maillette) during the summer of 2018. Plants were grown from 1-year-old cuttings provided by a lavender producer in Les-granges-Gontardes (44°24′57.24″ N, 4°45′47.304″E, 100 m a.s.l). In January 2018, eight plants were potted in 10 liter pots filled with 5.7 kg of soil recommended for aromatic plant cultivation (Klasmann code 693: medium fibrous structure, pH 6.0 ± 0.3, mainly composed of blond sphagnum peat and coconut fibers for optimal ventilation) and grown in a greenhouse for 6 months where they were watered daily at field capacity. All eight plants were similar with respect to their morphology (height, architecture, and leaf density). Temperature and relative humidity were monitored in the greenhouse, and the cooling system started when the temperature reached 35 °C.

Dehydration treatment

Eight plants were dehydrated until extreme desiccation, as described in Lamacque *et al.* (2020). Plants were uprooted, put in a temperature-controlled chamber at constant temperature (25 °C) and light levels (two lights of 25 W and 172 lm), and dehydrated until the stem diameter remained constant for at least 24 h; no AEs were recorded within this period. The typical duration of the experiment was ~10 d.

Acoustic emission analysis

AEs were recorded using a PCI2 system (Physical Acoustics, PAC18-bit A/D, 1 kHz–3 MHz) or a Samos system (1–400 kHz) connected to broad range acoustic sensors (150–800 kHz ISD9203B) through a pre-amplifier set to 40 dB. One sensor per individual was directly mounted on a branch where the bark was removed along ~2 cm. The debarked surface was covered with silicone grease to prevent further water loss and optimize acoustic coupling. The sensor was tightly clamped to the debarked part of the sample. The acoustic detection threshold was set to 40 dB. Acoustic coupling was tested using the Hsu–Nielsen method (lead break; Kalyanasundaram *et al.*, 2007; Charrier *et al.*, 2014b) at a distance of 1 cm from each sensor, and sensors were reinstalled when the signal amplitude was <75 dB. AE analyses were performed using AEwin software (Mistras Holdings). Acoustic activity was calculated as AE min^{-1} (averaged across 6 min). Five plants were analyzed using the Samos system and five using the PCI2 system. For a technical repetition, two plants were connected to both Samos and PCI2 systems, on two different branches. The experimental device is represented in Supplementary Fig. S1.

Each acoustic wave was analyzed by the AEwin software, and nine relevant characteristics were extracted from the original signal (amplitude, Amp; Energy; absolute energy, Abs Energy; signal strength, Sig Strength; rise angle; duration; rise time; counts to peak, P Count; and counts). The acoustic wave was also transformed using fast Fourier transform to compute six frequency-related characteristics (average frequency, A Frq; frequency centroid, C Frq; initiation frequency, I Frq; peak frequency, P Frq; reverberation frequency, R Frq; and weighed peak frequency, WPF).

Monitoring of branch diameter variations

Branch diameter was continuously measured using miniature displacement sensors with a friction-free core glued to the bark (Supplementary Fig. S1) and a linear variable differential transformer (LVDT; model DF2.5 and DF5.0; Solartron Metrology, Massy, France) connected to a wireless PepiPIAF system (Capt-connect, Clermont-Fd, France). Straight and unbranched sections of main branches longer than 5 cm were randomly chosen to mount LVDT dendrometers by a custom-made stainless Invar (alloy with minimal thermal expansion) holder adapted for lavender. At the end of the dehydration, the final branch diameter was measured using a calliper (Burg Wächter, 0.01 mm accuracy) at the location of the friction-free core of the LVDT dendrometer measurement. One LVDT per individual lavender was mounted, and branch diameter was recorded at 5 min intervals until the end of the experiment.

The percentage loss of diameter (PLD) was calculated from branch diameter variation during drought stress, according to Lamacque *et al.* (2020) for each plant as:

$$\text{PLD} = 100 \times \frac{D_{max} - D_{min}}{D_{max}} \tag{1}$$

where D_{max} and D_{min} are the maximum (before the dehydration) and the minimum (at the end of the dehydration) branch diameter, respectively.

Water potential

Water potential was measured regularly over the course of the dehydration using a Scholander-type pressure chamber (PMS Instrument, Albany, OR, USA). Measurements were carried out on ~5–10 cm long upper branch segments bearing several leaves. For each kinetic point, measurements were performed on each plant three times.

Xylem embolism

Measurements of loss of hydraulic conductance were performed before the plants were uprooted and then two or three times during dehydration. Xylem embolism on stems was measured using a xylem embolism meter (XYL'EM, Bronkhorst, Montigny-les-Cormeilles, France). The entire inflorescence stems of ~30 cm long were collected and put in wet black plastic bags, and then brought immediately to the laboratory for measurements. Segments of 5 cm were cut under water and fitted to water-filled tubing. One end of the stem inflorescence segment was connected to a tank of de-gassed, filtered 10 mM KCl and 1 mM CaCl$_2$ solution. The flux of the solution was recorded through the stem section under low pressure (60–90 mbar) and the initial hydraulic conductance (K_i) scored. The stem was perfused at least twice for 10 s then 2 min at 1 bar until the hydraulic conductance no longer increased in order to remove air from embolized vessels and to determine the maximum conductance (K_{max}). The percentage loss of hydraulic conductance (PLC) was determined as:

$$PLC = 1 - \frac{K_i}{K_{max}} \tag{2}$$

PLC was measured on each individual plant with at least three repetitions for each individual.

In addition, the PLC of three different branches (woody and inflorescence stems) was determined by using X-ray microcomputed tomography (micro-CT), a technique that allows direct observation of embolized or non-embolized vessels (Choat *et al.*, 2016). Thus, each branch was adjusted to 5 cm length with a razor blade, immersed in wax to avoid dehydration during scanning, and placed in an X-ray microtomograph (Nanotom 180 XS, GE, Wunstorf, Germany) at the PIAF laboratory (INRAE, Clermont-Ferrand, France). For the micro-CT image acquisition and image combination, the field of view was adjusted to 5.1 × 5.1 × 5.1 mm^3 and the X-ray source set to 60 kV and 240 μA. For each ~21 min scan, 1000 images were recorded during the 360° rotation of the sample. The microtomography scans were reconstructed in three-dimensions (3D) with a spatial resolution of 2.5 μm per voxel and one transverse 2D slice was extracted from the middle of the volume using Phoening datosx 2 software (General Electric, Boston, MA, USA). After the first scan of the sample, the sample was cut in the air just below the scanned area and a second scan was performed. The cut induced entrance of air into the functional conduits which allows measurement of all the functional conduits of the sample. PLC was then calculated by comparing the area occupied by embolized vessels measured during the first scan (Ae) and after the cut (corresponding to the total xylem conductivity area (Ac) as:

$$PLC = \frac{Ae}{Ac} \tag{3}$$

PLC determined by using micro-CT was measured at three critical times during the dehydration: before the start of dehydration, after the first peak of AEs, and after the second peak of AEs, in order to validate the results obtained with the XYL'EM.

Electrical conductivity

To assess drought-induced cellular damage, the relative electrical conductivity (REC), based on electrolyte leakage, was measured three times during dehydration. Samples 5 cm long were cut into 5 mm long sections and immersed into 15 ml of distilled-deionized water. Vials were shaken for 24 h at +5 °C in the dark (to limit bacterial growth) on a horizontal gravity shaker (ST5, CAT, Staufen, Germany). The electric conductivity of the solution was measured (C_1) at room temperature using a conductimeter (Held Meter LF340, TetraCon® 325, Weiheim,

Germany). After autoclaving at +120 °C for 30 min and cooling down to room temperature, the conductivity was measured again (C_2). REC was calculated as:

$$REL = \frac{C_1}{C_2} \times 100 \tag{4}$$

To normalize the REC, 10 control samples (i.e. well-watered WW) and 10 frozen samples (–80 °C) were used to have a reference for 0% (REC$_{WW}$) and 100% cellular damage (REC$_{-80}$), respectively. An index of damage, I$_{Dam}$, was computed as:

$$I_{Dam} = \frac{REC - REC_{WW}}{REC_{-80}} \tag{5}$$

Statistical analysis

Statistical analyses were performed using the RStudio software (under R core version 4.0.3, R Core Team, 2020). The nls function was used to fit the relationships among PLC, I$_{dam}$, ψ, and PLD. The parameters of acoustic emissions were analyzed by principal component analysis (PCA), using the pca function (FactoMineR package). The Kaisier–Mayer–Olkin index (KMO) was calculated to measure the adequacy of the dataset for PCA (Kaiser, 1974). This test measures whether each variable has a proportion of its variance that is common to the other variables. In our dataset, the KMO index was 0.652, which indicates that each variable has a sufficient proportion of its own variance and is therefore adequate for PCA. As the variables had very different orders of magnitude, they were centered and scaled before PCA. Following the PCA, latent variables, which are variables that cannot be measured directly, but are inferred from the observed variables, were computed as the linear combination of observed variables:

$$LV_n = \sum_{i=1}^{16} \frac{x_i - \bar{x}}{\sigma} \cdot P_n \tag{6}$$

where LV$_n$ represents the latent variable of dimension n, xi, $\bar{x}$, and σ the value, the mean, and the SD of the acoustic variable I, and P$_{n,i}$ the coefficient for the dimension n and the acoustic variable i.

Results

During dehydration, lavender plants exhibited two distinct phases of high acoustic activity (>1 AE min^{-1}) clearly separated in time by a relatively less active phase (Fig. 1). The first phase occurred during a strong decrease in diameter, whereas during the second phase, the decrease in diameter was much lower, reaching almost steady-state values. The highest activities during the two phases (AE$_1$ and AE$_2$) occurred at a relatively similar PLD across plants: 11.75 ± 0.84 and 22.26 ± 1.10% PLD for AE$_1$ and AE$_2$, respectively, and were different between the phases (*P*<0.001; Supplementary Fig. S2). The first phase of AEs was very similar and lasted <100 h in all plants using either recording system, Samos or PCI2 (Fig. 1; Supplementary Figs S3, S4). In contrast, a greater variability in duration and peak activity was observed for the second phase of AEs.

During the two periods of intense acoustic activity, loss of hydraulic conductivity (PLC) and the index of cellular damage (I$_{Dam}$) increased independently (Fig. 2A, B).
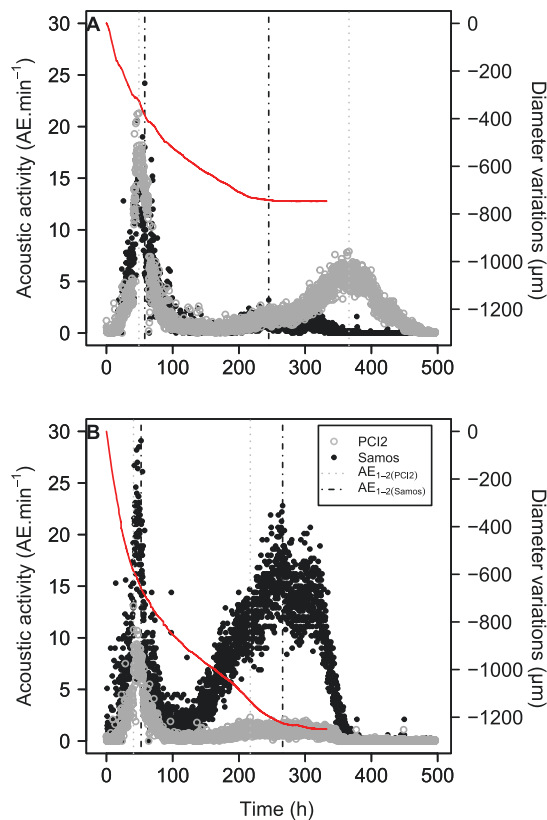
Fig. 1. Acoustic activity and diameter change in two dehydrating lavender plants. (A and B) Acoustic activity (acoustic events per minute; black dots) and change in branch diameter (red lines) during dehydration of two different uprooted lavender plants under constant temperature (25 °C). Two acoustic recording systems were used for each plant: PCI2 (gray points) and Samos (black points). The dotted lines represent the time at highest peak acoustic activity for two phases (AE_1 and AE_2). The other acoustic records are presented in Supplementary Figs S3 and S4.

After the first acoustic phase, PLC reached $87.32 \pm 3.61\%$ and I_{Dam} $47.22 \pm 10.03\%$. After the second acoustic phase, PLC remained high ($97.37 \pm 1.14\%$), while I_{Dam} reached $75.37 \pm 9.31\%$. Depending on the PLD, PLC and I_{Dam} both fit a sigmoidal function (pseudo-r^2=0.85 and 0.75 for PLC and I_{Dam}, respectively; Lamacque *et al.*, 2020). The water potential decreased with increasing PLD according to an exponential model (pseudo-r^2=0.46, Fig. 2B), reaching values lower than −9 MPa (i.e. minimum measurable water potential) after AE_2.

The contrasted dynamics in PLC and I_{dam} suggest that two distinct acoustic phases may result from different phenomena. The variability across extracted characteristics from each AE recorded using a PCI2 recording system was explored through multivariate PCA with respect to acoustic phase (Fig. 3A; Supplementary Fig. S2). The five first components contributed to 78% of cumulated variance (from 33% to 7% for each component; Table 1). Dimensions 1 and 2 of the PCAs reflected 50% of the total variance in acoustic parameters. Signal strength, energy, counts, and duration of the acoustic event mainly contributed to the first component (dimension

1, Dim_1; Supplementary Table S1). Frequency–related parameters, with the exception of the initiation frequency, mainly contributed to the second component (Dimension 2, Dim_2; Supplementary Table S1). However, Dim_1 and Dim_2 did not highlight any difference across acoustic phases (see Supplementary Fig. S5). We explored the residual information contained in the other dimensions. Dimensions 3 and 4 accounted for 20% of the variance. Absolute energy and parameters related to the beginning of the AE (initiation frequency, rise time, and rise angle) mainly contributed to the third component (Dimension 3, Dim_3; Fig. 3B; Supplementary Table S1). Initiation frequency, rise angle, average frequency, and counts to peak mainly contributed to the fourth component (Dimension 4, Dim_4). According to Dim_3 and Dim_4, acoustic phases were discriminated from top left to bottom right (along the $y=-x$ line, Fig. 3A). Signals from AE_1 were located all along this line, whereas signals from AE_2 were only located in the top left quarter [i.e. positive latent variable 3 (LV_3) and negative latent variable 4 (LV_4) with respect to Dim_3 and Dim_4, respectively; Fig. 3A]. Considering that vessels were fully embolized after AE_1, we assumed that hydraulically related signals were not generated during AE_2 and therefore were located in the lower right quadrat. Other sources were located in the top left quadrat. More precisely, thresholds in LV_3 and LV_4 were defined based on their distribution for AE_2 signals. To exclude outliers, the 99th percentile in LV_3 (1.4) and the first percentile in LV_4 (−2.5) were used as thresholds to define acoustic sources: the source was considered to be from a hydraulic origin if $LV_3 >1.4$ and $LV_4 < -2.5$. If not, the source was considered as non-hydraulic. Hydraulically related AEs represented 16.65% of the total population of signals (~68 000 over 410 000 recorded AEs). A sigmoidal function described the relationship between hydraulically related events and loss of diameter, with PLD_{50} equal to $11.1 \pm 0.3\%$ (Fig. 4A). Thanks to the non-linear relationship (described in Fig. 2B), the water potential inducing 50% of cavitation events was computed as $\Psi_{AE50}= -4.2 \pm 0.3$ MPa (the water potential inducing 50% of cavitation events determined via AEs; Fig. 4B).

The algorithm developed from the PCI2 system was applied to the signals recorded from another ultrasound acoustic system (Samos). As observed with signals from PCI2, filtered acoustic emissions fit the same pattern in response to loss of diameter with a similar PLD_{50} (PLD_{50}=11.4 ± 3.9%; Fig. 4C). The PLD values of phases 1 and 2 were not significantly different between the two recording systems Samos and PCI2 (P=0.21 and 0.67, respectively). With respect to water potential, Ψ_{AE50} was also similar to that computed with PCI2 signals: $\Psi_{AE50}= -4.4 \pm 0.4$ MPa (Fig. 4D). Finally, the vulnerability curves derived from both acoustic systems overlapped with no significant inflexion points (P=0.65) and slopes (P=0.2; Fig. 5). However, the water potential inducing 50% loss of hydraulic conductance, $\Psi_{PLC50}= -2.54 \pm 0.2$ MPa, was significantly higher than those based on acoustic activities (P<0.001).
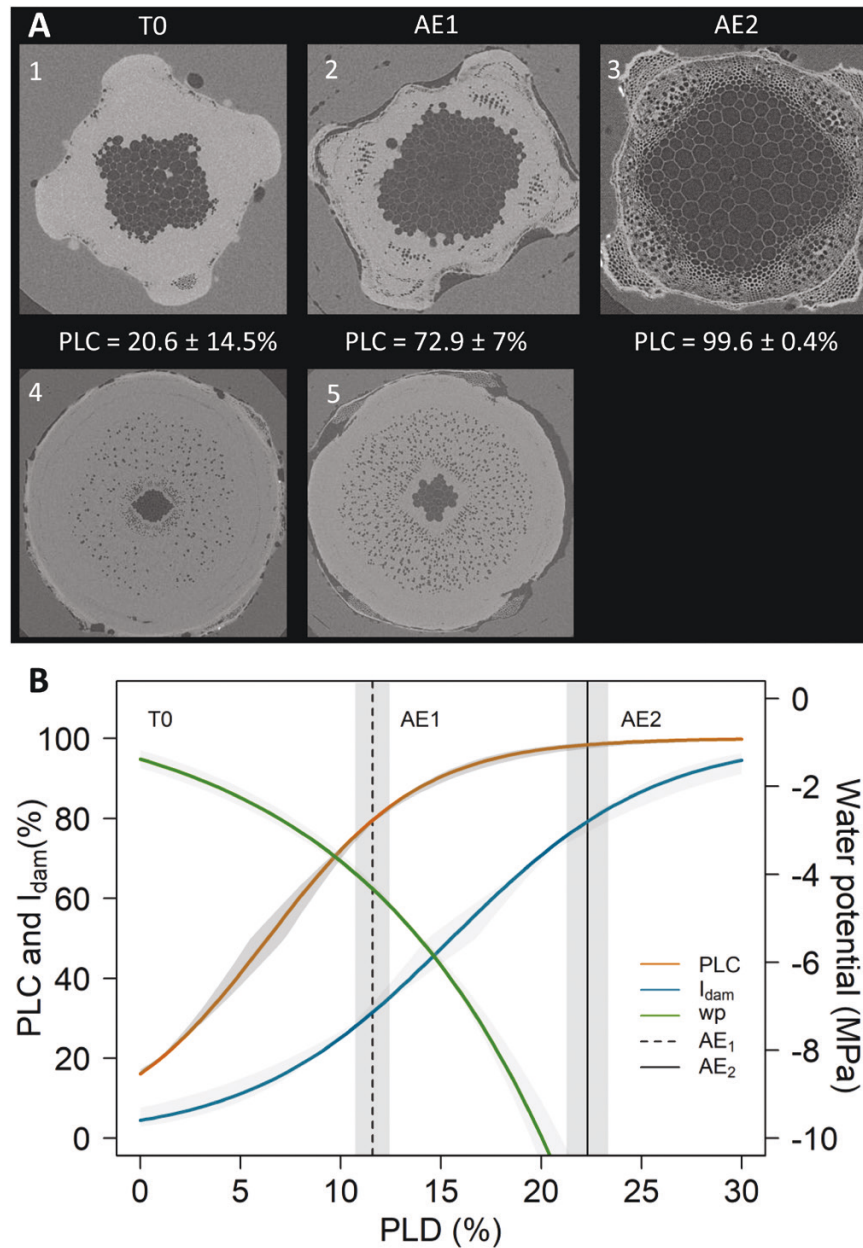
Fig. 2. Water potential, embolism formation, and cellular damage depending on stem shrinkage (A) Transverse section of inflorescence stems (1–3) and branches (4–5) by high resolution computed tomography at three phases during dehydration: initial phase (T$_0$; Ψ= −1.05 ± 0.12 MPa), after the first peak of acoustic emissions (AE$_1$; Ψ= −4.4 ± 0.03 MPa), and after the second peak of acoustic emissions (AE$_2$; Ψ< −9 MPa). Dark areas represent low-density areas (i.e embolized vessels and pith). PLC is the loss of xylem hydraulic conductivity for each phase (mean ±SE from *n*=3 for T$_0$ and AE$_2$, and *n*=5 for AE$_1$). (B) PLC, water potential, and relative cellular damage measured by the electrolyte leakage method (I$_{dam}$) depending on percentage loss of diameter (PLD) during dehydration. PLDs at AE$_1$ and AE$_2$ are represented by vertical dotted and black lines, respectively (SE in shaded area). See Lamacque *et al.* (2020) for further explanations.

Filtered out signals (i.e. negative LV$_3$ or positive LV$_4$), called non–hydraulic AEs, exhibited much higher variability across replicates than filtered signals in relation to PLD or Ψ (Fig. 6). However, the dynamics of these signals were consistent between both recording systems PCI2 and Samos (*P*=0.47) and with the increase in cellular damage measured by electrolyte leakage (Fig. 6, *P*=0.13).

Discussion

Two acoustic phases related to two mechanisms

The detection of distinct phases of AEs while monitoring continuous stem diameter provided an exceptional opportunity to discriminate between hydraulic-related AEs and other sources to monitor drought-induced damage, namely cavitation and
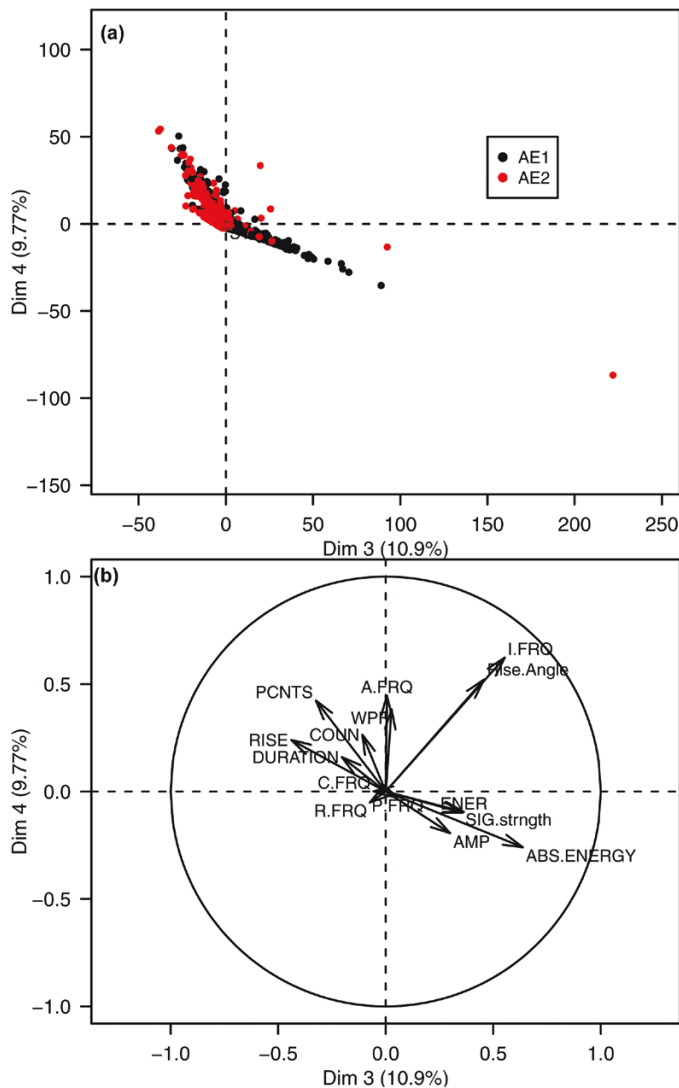
Fig. 3. Principal component analysis performed on acoustic signals. (A) Principal component analysis (PCA) based on characteristics of recorded acoustic emission during dehydration of uprooted lavender with the PCI2 system. Black and red dots represent the signals recorded during distinct acoustic phase (AE_1 and AE_2, respectively). Dimensions 3 and 4 are represented as they maximize the discrimination between AE_1 and AE_2 (the other combinations are represented in Supplementary Fig. S1). (B) Contribution of each acoustic characteristic to Dim 3 and 4.

suggest that most signals corresponding to cavitation events were recorded during AE_1. However, cellular damage was also increasing during AE_1; thus not only cavitation events are likely to be recorded during this phase.

During the second phase, AE_2, since the shrinkage goes on and the branch becomes completely dry, events other than cavitation such as cracks (De Roo *et al.*, 2016) or cell wall shrinkage (Čunderlik *et al.*, 1996) are likely to generate AEs. The relationship with cellular damage is not straightforward, although frost-induced cellular damage has been shown to induce AEs (Kasuga *et al.*, 2015). The correlation between AEs and cellular damage can be explained by different processes such as membrane rupture, intracellular cavitation, or wall cracks (Sakes *et al.*, 2016). For the second phase, the signals did exhibit much higher variability across plants and acoustic systems, suggesting that the source of these signals may be multiple, although probably including cellular damage (Fig. 6).

Another study also showed distinct acoustic phases in relation to stem shrinkage and cavitation events, respectively (Vergeynst *et al.*, 2014). However, in our study, AEs were recorded over a much wider range of drought stress, well beyond the threshold for hydraulic failure and cellular damage (Ψ < −9 MPa), although branch shrinkage continued during the dehydration experiment. As plant mortality ensues, membrane rupture or intracellular cavitation is likely to happen (Sakes *et al.*, 2016). As cellular damage and mechanical constraints may be generated over the whole dehydration process and can induce AEs, we suggest that these signals were recorded during both acoustic phases.

Can we use acoustic signals to construct vulnerability curves?

Considering that vessels were fully embolized after AE_1, we assumed that hydraulically related signals were not generated during AE_2. The PCA used on the parameters of the population of AEs allowed discrimination of AEs related to hydraulic failure from the other sources and could therefore help to build vulnerability curves.

The first two principal components (Dim_1 and Dim_2) did not allow any discrimination across acoustic phases. We suggest that the parameters contributing significantly to these two principal components were mainly related to the structure of the plant tissue and driven by attenuation properties within plant tissue. The sources of AEs are distributed within the sample and propagate from different locations towards the sensor through the tissues. During the propagation, signals are attenuated, differentially depending on the frequency. Signal shape and the parameters of acoustic waves will therefore change depending on the distance between the source and the sensor. We thus hypothesized that the first two dimensions of the PCA, accounting for 50% of the total variance (Table 1), were mainly affected by the differential attenuation depending on the distance to the source. The main variables explaining

cellular damage (Fig. 1). A single phase of AE is usually recorded during dehydration (Rosner et al., 2006, 2009). However, beyond the peak in acoustic activity, numerous emissions were recorded following a long tailed distribution (Wolkerstorfer *et al.*, 2012; Nolf *et al.*, 2015). In the present study, the first phase of AEs, AE_1, occurred during the main and rapid shrinkage of the stem, while the second phase occurred when the diameter change became lower (Supplementary Figs S6, S7). The transition between the two acoustic phases corresponded to a breakpoint of diameter change at PLD 10–15% while xylem embolism was almost total (PLC >90%; Fig. 2). We therefore

Table 1. Principal component analysis performed on acoustic characteristics of signals recorded during dry-down of lavender

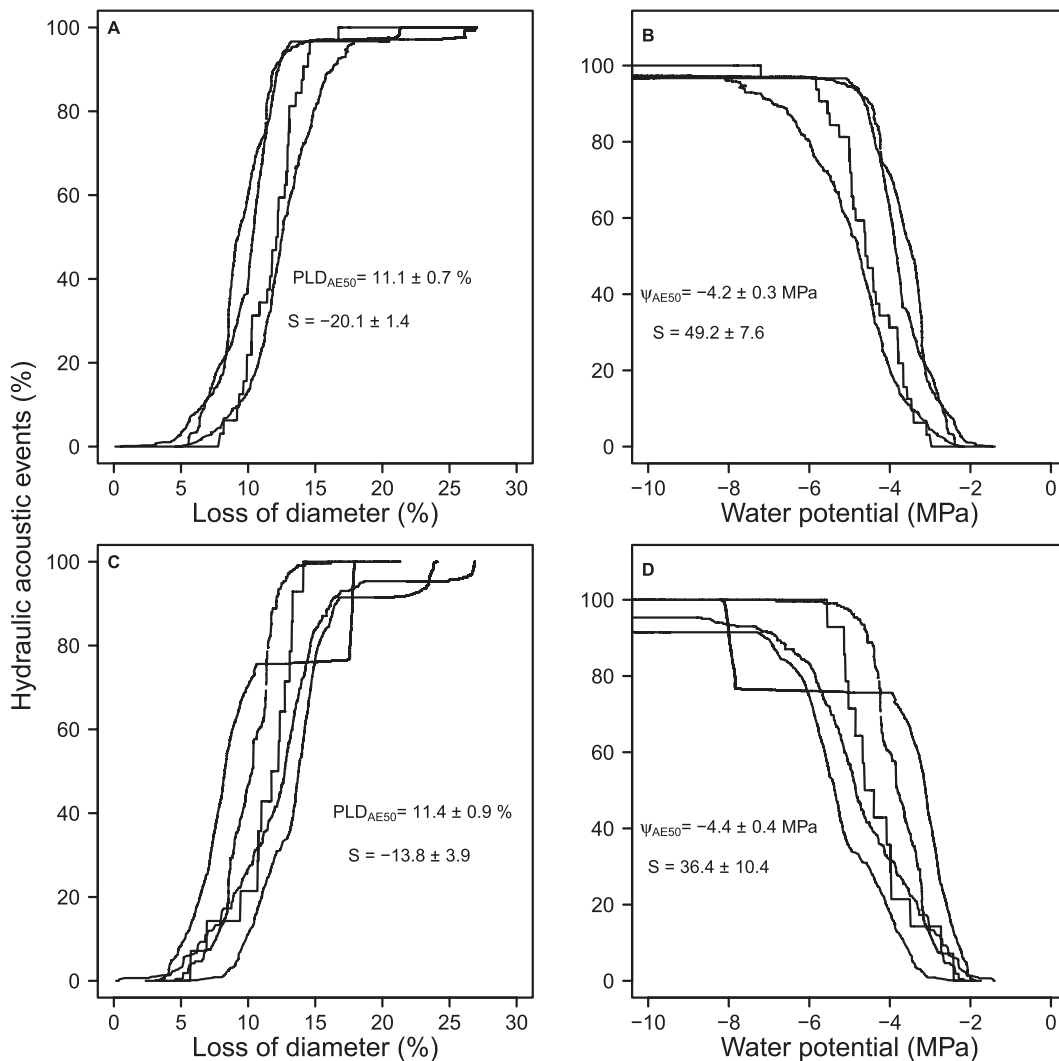| Dimension	Variance	Variance (%)	Cumulated variance
1	4.9	33.3	33.3
2	2.56	17.1	50.3
3	1.64	10.9	61.2
4	1.47	9.8	71.0
5	1.05	7.0	78.0
6	0.91	6.1	84.0
7	0.66	4.4	88.4
8	0.56	3.8	92.2
9	0.46	3.1	95.3
10	0.27	1.8	97.1
11	0.22	1.4	98.5
12	0.15	1.0	99.5
13	0.08	0.5	100
14	0	0	100
15	0	0	100

Fig. 4. Acoustic-based hydraulic vulnerability curves. Cumulated hydraulically related acoustic events based on Dimensions 3 and 4 depending on the percentage loss of diameter (PLD; A and C) and the water potential (B and D). Upper and lower panels represent the signals recorded by the PCI2 and Samos recording systems, respectively.
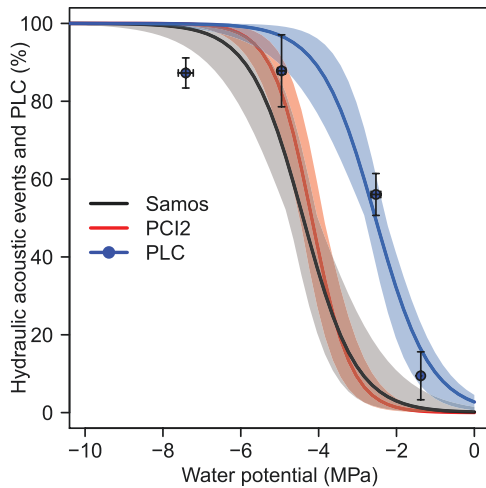
Fig. 5. Comparison of hydraulic and acoustic vulnerability curves. Cumulated hydraulically related acoustic events from two independent recording systems, PCI2 (black line) and Samos (red line), and loss of hydraulic conductance measured on branches (blue points and line). Shaded areas represent SEs.
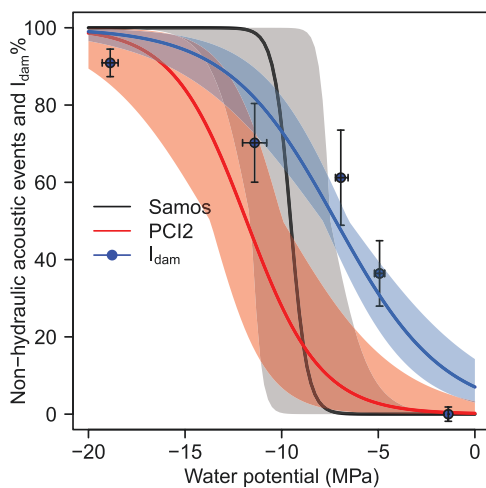

Fig. 6. Comparison of cellular damage and acoustic vulnerability curves. Non-hydraulic acoustic events from two independent recording systems, PCI2 and Samos, in black and red, respectively. Relative cellular damage measured by the electrolyte leakage method (I_{dam}) during dehydration are represented in blue. Shaded areas represent SEs.

the first two components were indeed more likely to be affected by the propagation within the xylem (energy, count, duration, amplitude, average frequency, etc.).

The third and fourth principal components (Dim_3 and Dim_4) did allow a clear distinction between the two acoustic phases AE_1 and AE_2. The variables explaining Dim_3 and Dim_4 (initiation frequency, peak frequency, rise time, and rise angle) are less likely to be attenuated by the wood matrix and thus should be more tightly correlated to the source. Graphically, Dim_3 and Dim_4 discriminated the AEs generated during AE_1 and AE_2, and still accounted for 21% of the total variance

(Fig. 3). As all the signals corresponding to cavitation events were recorded during AE_1, we suggest that the signals of positive LV_3 and negative LV_4 are generated by cavitation events. The simple rule ($LV_3 > 1.4$ and $LV_4 < -2.5$) was used to reconstruct a vulnerability curve based on acoustic emissions. Vulnerability curves reconstructed with AEs showed similar results between the two acoustic recording systems PCI2 and Samos, which have different frequency ranges (1 kHz–3 MHz and 1–400 kHz, respectively) with $\Psi_{AE50} = -4.1 \pm 0.3$ MPa and -4.3 ± 0.3 MPa (Figs 4, 5). The curves based on diameter loss are also very similar across systems, with very close PLD_{50} (~11%; Fig. 4). Testing the decision rules with an independent recording system provided a similar vulnerability index (Ψ_{AE50} and slopes) in the same and in independent individual plants.

The hydraulic vulnerability reported with this method is lower than Ψ_{PLC50} acquired using hydraulic methods (approximately −2.5 MPa; Lamacque *et al.*, 2020, *P*<0.001). The PLC curve is based on real hydraulic measurements (i.e. flow measured in the stem) and is therefore affected by the number of embolized vessels, whereas the acoustic curve, based on filtered AEs, can be generated by cavitation in conduits and air seeding through pit membranes. Even if each single event would represent exactly one cavitation event in a conduit (Tyree and Dixon, 1983; Tyree *et al.*, 1984), the relationship between cumulative AEs and conductivity loss will be non-linear if not all the xylem elements individually contribute equally to the total hydraulic conductivity (Cochard, 1992). The impact of an embolized vessel on the conductance would vary greatly depending on the vessel dimensions, the xylem network, and the level of xylem embolism. Within the xylem, the larger vessels are embolized earlier than smaller ones (Lemaire *et al.*, 2021). The first cavitation events therefore have a greater effect on conductance than the last ones, so that the loss of conductance is very high when half the vessels are embolized. This might explain why the water potential inducing 50% of cavitation events (Ψ_{AE50}) would be lower than that inducing 50% loss of conductance (Ψ_{PLC50}). Furthermore, the water potential was not measured continuously but regularly during dehydration. To represent the AEs as a function of water potential, we used the non-linear relationship found between Ψ and PLD. However, this translation is only an estimate, and an uncertainty in the computed Ψ values remains. This could contribute to the discrepancy between Ψ_{AE50} and Ψ_{PLC50}. Similar experimentation with higher frequency in the Ψ measurements could help mitigate such a difference.

The lavenders used in this study were rather vulnerable to cavitation compared with other Mediterranean shrub species (Lamacque *et al.*, 2020). Since plasticity was reported for this trait (Awad *et al.*, 2010; Herbette *et al.*, 2010), we assume that the lavender plants grown under well-watered conditions have developed more hydraulically vulnerable xylem, whereas other parameters related to cellular damages or fractures may not have exhibited such a plasticity. These particular conditions

would explain why two distinct acoustic phases were observed while plants grown in the field would have exhibited overlapped AE phases (Nolf *et al.*, 2015).

AE$_2$ as an indicator of mortality

All of the variables measured here (i.e. branch diameter, acoustic events, loss of hydraulic conductance, water potential, and cellular damage) helped to characterize the plant's response to water stress. Monitoring the variations in branch diameter allows determination of the threshold of mortality. In addition, measurements are still possible under extreme stress up to the point where water potential is no longer measurable, namely when petioles are fully embolized and very little free water remains in the plant xylem (Lamacque *et al.*, 2020). In lavender, the percentage loss of diameter corresponding to a complete loss of rehydration capacity (PLRC) was equal to 21.3% (Lamacque *et al.*, 2020).

Here, AE$_1$ and AE$_2$ peaks were recorded on average for PLD=11.7% and 22.3%, respectively (Fig. 2). Based on the reported relationship between PLD and PLRC (Lamacque *et al.*, 2020), AE$_1$ and AE$_2$ would be associated with 30.2% and 98.1% PLRC, respectively. Hydraulic failure, determined through the AE$_1$ phase, is thus not a relevant signal for plant mortality even though it could lead to plant mortality through the complete desiccation of the meristematic cells (Lamacque *et al.*, 2020; Mantova *et al.*, 2021). The assessment of cellular damage is thus highly relevant to predict plant mortality under extreme drought (Vilagrosa *et al.*, 2010; Guadagno *et al.*, 2017). The detection of AE$_2$ emissions would therefore be a relevant signal to detect plant mortality. It is also supported by the seasonal dynamics in acoustic activity in relation to the freezing resistance of living cells in the same species (Charrier *et al.*, 2021b). Plant recovery was not measured in the present study, although the plant material is similar to that used in Lamacque *et al.* (2020).

Conclusions

Two distinct phases of AEs were recorded during the complete dehydration of lavender. Each phase had a particular acoustic signature, highlighted by the PCA method, and was related to successive drought-induced damage: xylem hydraulic failure and cellular damage. Hydraulic failure happened much earlier than cellular damage, the latter being tightly linked to the stability of branch diameter that can be reached more rapidly after xylem hydraulic failure. By combining different measurements, this study helped to clarify the dynamics of drought-induced damage. It provides avenues for future research by proposing a new way to reconstruct xylem vulnerability curves from the non-invasive analysis of AEs generated by cavitation events. This method deserves to be tested in other species to assess whether two acoustic phases would be recorded.

Supplementary data

The following supplementary data are available at *JXB* online.

Fig. S1. (A) Experimental set-up in the temperature-controlled chamber, combining LVDT and the acoustic sensor. (B) Zoom in on the acoustic sensor.

Fig. S2. Acoustic activity depending on percentage loss of diameter.

Fig. S3. Acoustic activity recorded by the Samos system and change in branch diameter during dehydration of different uprooted lavender plants under constant temperature (25 °C).

Fig. S4. Acoustic activity recorded by the PCI2 system and change in branch diameter during dehydration of different uprooted lavender plants under constant temperature (25 °C).

Fig. S5. Different combinations of the four first dimensions of the principal component analysis based on characteristics of recorded acoustic emission during dehydration of uprooted lavender with the PCI2 system.

Fig. S6. Acoustic activity and change in branch diameter during dehydration. A segmented regression indicates the significant change in the slope of the diameter during dehydration.

Fig. S7. Maximum acoustic activity depending on the slopes of diameter variations.

Table S1. Description of acoustic parameters based on PCA and contribution to latent variables 1–5.

Data availability

The data that support the findings of this study are available from the corresponding author upon reasonable request.

References

Améglio T, Cochard H, Ewers FW. 2003. Gelista™: a new tool for testing frost hardiness by stem diameter variations on walnut. Acta Horticulturae **618**, 509–514.

Anderegg WRL, Klein T, Bartlett M, Sack L, Pellegrini AFA, Choat B, Jansen S. 2016. Meta-analysis reveals that hydraulic traits explain cross-species patterns of drought-induced tree mortality across the globe. Proceedings of the National Academy of Sciences, USA **113**, 5024–5029.

Awad H, Barigah T, Badel E, Cochard H, Herbette S. 2010. Poplar vulnerability to xylem cavitation acclimates to drier soil conditions. Physiologia Plantarum **139**, 280–288.

Barigah TS, Charrier O, Douris M, Bonhomme M, Herbette S, Améglio T, Fichot R, Brignolas F, Cochard H. 2013. Water stress-induced xylem hydraulic failure is a causal factor of tree mortality in beech and poplar. Annals of Botany **112**, 1431–1437.

Brodribb TJ, Carriqui M, Delzon S, Lucani C. 2017. Optical measurement of stem xylem vulnerability. Plant Physiology **174**, 2054–2061.

Brodribb TJ, Cochard H. 2009. Hydraulic failure defines the recovery and point of death in water-stressed conifers. Plant Physiology **149**, 575–584.

Brodribb TJ, Skelton RP, McAdam SAM, Bienaimé D, Lucani CJ, Marmottant P. 2016. Visual quantification of embolism reveals leaf vulnerability to hydraulic failure. New Phytologist **209**, 1403–1409.

Charra-Vaskou K, Badel E, Charrier G, Ponomarenko A, Bonhomme M, Foucat L, Améglio T. 2016. Cavitation and water fluxes driven by ice water potential in *Juglans regia* during freeze–thaw cycles. Journal of Experimental Botany **67**, 739–750.

Charra-Vaskou K, Charrier G, Wortemann R, Beikircher B, Cochard H, Ameglio T, Mayr S. 2012. Drought and frost resistance of trees: a comparison of four species at different sites and altitudes. Annals of Forest Science **69**, 325–333.

Charrier G, Améglio T. 2011. The timing of leaf fall affects cold acclimation by interactions with air temperature through water and carbohydrate contents. Environmental and Experimental Botany **72**, 351–357.

Charrier G, Améglio T, Herbette S, Lamacque L, Sabin F, Serre C, Wielemans A. 2021b. Detecting cellular damages in freezing plants: are acoustic emissions useful? In: 2021 IEEE International Workshop on Metrology for Agriculture and Forestry (MetroAgriFor). IEEE, 140–144.

Charrier G, Charra-Vaskou K, Kasuga J, Cochard H, Mayr S, Améglio T. 2014b. Freeze–thaw stress: effects of temperature on hydraulic conductivity and ultrasonic activity in ten woody angiosperms. Plant Physiology **164**, 992–998.

Charrier G, Charra-Vaskou K, Legros B, Améglio T, Mayr S. 2014a. Changes in ultrasound velocity and attenuation indicate freezing of xylem sap. Agricultural and Forest Meteorology **185**, 20–25.

Charrier G, Martin-StPaul N, Damesin C, *et al*. 2021a. Interaction of drought and frost in tree ecophysiology: rethinking the timing of risks. Annals of Forest Science **78**, 40.

Charrier G, Nolf M, Leitinger G, Charra-Vaskou K, Losso A, Tappeiner U, Améglio T, Mayr S. 2017. Monitoring of freezing dynamics in trees: a simple phase shift causes complexity. Plant Physiology **173**, 2196–2207.

Choat B, Badel E, Burlett R, Delzon S, Cochard H, Jansen S. 2016. Noninvasive measurement of vulnerability to drought-induced embolism by X-ray microtomography. Plant Physiology **170**, 273–282.

Cochard H. 1992. Vulnerability of several conifers to air embolism. Tree Physiology **11**, 73–83.

Cochard H, Delzon S, Badel E. 2015. X-ray microtomography (micro-CT): a reference technology for high-resolution quantification of xylem embolism in trees. Plant, Cell & Environment **38**, 201–206.

Čunderlik I, Moliński W, Raczkowski J. 1996. The monitoring of drying cracks in the tension and opposite wood by acoustic emission and scanning electron microscopy methods. Holzforschung-Wood Research and Technology **50**, 258–262.

Daudet F-A, Améglio T, Cochard H, Archilla O, Lacointe A. 2004 Experimental analysis of the role of water and carbon in tree stem diameter variations. Journal of Experimental Botany **56**, 135–144.

De Roo L, Vergeynst LL, De Baerdemaeker NJF, Steppe K. 2016. Acoustic emissions to measure drought-induced cavitation in plants. Applied Sciences **6**, 1–15.

Dixon HH, Joly J. 1895. XII. On the ascent of sap. Philosophical Transactions of the Royal Society B: Biological Sciences **563**, 576.

Ennajeh M, Simões F, Khemira H, Cochard H. 2011. How reliable is the double-ended pressure sleeve technique for assessing xylem vulnerability to cavitation in woody angiosperms? Physiologia Plantarum **142**, 205–210.

Ganthaler A, Mayr S. 2015. Dwarf shrub hydraulics: two Vaccinium species (*Vaccinium myrtillus*, *Vaccinium vitis-idaea*) of the European Alps compared. Physiologia Plantarum **155**, 424–434.

Guadagno CR, Ewers BE, Speckman HN, Aston TL, Huhn BJ, DeVore SB, Ladwig JT, Strawn RN, Weinig C. 2017. Dead or alive? Using membrane failure and chlorophyll a fluorescence to predict plant mortality from drought. Plant Physiology **175**, 223–234.

Guàrdia M, Charrier G, Vilanova A, Savé R, Ameglio T, Aletà N. 2016. Genetics of frost hardiness in *Juglans regia* L. and relationship with growth and phenology. Tree Genetics & Genomes **12**, 83.

Hammond WM, Yu KL, Wilson LA, Will RE, Anderegg WRL, Adams HD. 2019. Dead or dying? Quantifying the point of no return from hydraulic failure in drought-induced tree mortality. New Phytologist **223**, 1834–1843.

Herbette S, Le Menn A, Rousselle P, Ameglio T, Faltin Z, Branlard G, Eshdat Y, Julien J-L, Drevet JR, Roeckel-Drevet P. 2005. Modification of photosynthetic regulation in tomato overexpressing glutathione peroxidase. Biochimica et Biophysica Acta **1724**, 108–118.

Herbette S, Wortemann R, Awad H, Huc R, Cochard H, Barigah TS. 2010. Insights into xylem vulnerability to cavitation in *Fagus sylvatica* L.: phenotypic and environmental sources of variability. Tree Physiology **30**, 1448–1455.

Kaiser MO. 1974. Kaiser–Meyer–Olkin measure for identity correlation matrix. Journal of the Royal Statistical Society **52**, 296–298.

Kalyanasundaram P, Mukhopadhyay CK, Rao SVS. 2007. Practical acoustic emission. Oxford: Alpha Science International Limited.

Kasuga J, Charrier G, Uemura M, Améglio T. 2015. Characteristics of ultrasonic acoustic emissions from walnut branches during freeze–thaw-induced embolism formation. Journal of Experimental Botany **66**, 1965–1975.

Lamacque L, Charrier G, dos Santos Farnese F, Lemaire B, Améglio T, Herbette S. 2020. Drought-induced mortality: branch diameter variation reveals a point of no recovery in lavender species. Plant Physiology **183**, 1638–1649.

Lemaire C, Quilichini Y, Brunel-Michac N, Santini J, Berti L, Cartailler J, Conchon P, Badel E, Herbette S. 2021. Plasticity of the xylem vulnerability to embolism in *Populus tremula × alba* relies on pit quantity properties rather than on pit structure. Tree Physiology **41**, 1384–1399.

Lewis AM. 1988. A test of the air-seeding hypothesis using sphagnum hyalocysts. Plant Physiology **87**, 577–582.

Li S, Lens F, Espino S, Karimi Z, Klepsch M, Schenk HJ, Schmitt M, Schuldt B, Jansen S. 2016. Intervessel pit membrane thickness as a key determinant of embolism resistance in angiosperm xylem. IAWA Journal **37**, 152–171.

Lo Gullo MA, Salleo S. 1992. Water storage in the wood and xylem cavitation in 1-year-old twigs of *Populus deltoides* Bartr. Plant, Cell & Environment **15**, 431–438.

Mai J, Herbette S, Vandame M, Kositsup B, Kasemsap P, Cavaloc E, Julien JL, Améglio T, Roeckel-Drevet P. 2009. Effect of chilling on photosynthesis and antioxidant enzymes in *Hevea brasiliensis* Muell. Arg. Trees - Structure and Function **23**, 863–874.

Mantova M, Herbette S, Cochard H, Torres-Ruiz JM. 2021. Hydraulic failure and tree mortality: from correlation to causation. Trends in Plant Science **1**, 11.

Martin-StPaul N, Delzon S, Cochard H. 2017. Plant resistance to drought depends on timely stomatal closure. Ecology Letters **20**, 1437–1447.

Mayr S, Rosner S. 2011. Cavitation in dehydrating xylem of *Picea abies*: energy properties of ultrasonic emissions reflect tracheid dimensions. Tree Physiology **31**, 59–67.

Milburn JA, Johnson RPC. 1966. The conduction of sap. Planta **69**, 43–52.

Nardini A, Battistuzzo M, Savi T. 2013. Shoot desiccation and hydraulic failure in temperate woody angiosperms during an extreme summer drought. New Phytologist **200**, 322–329.

Nolf M, Beikircher B, Rosner S, Nolf A, Mayr S. 2015. Xylem cavitation resistance can be estimated based on time-dependent rate of acoustic emissions. New Phytologist **208**, 625–632.

Nolf M, Lopez R, Peters JMR, Flavel RJ, Koloadin LS, Young IM, Choat B. 2017. Visualization of xylem embolism by X-ray microtomography: a direct test against hydraulic measurements. New Phytologist **214**, 890–898.

Petruzzellis F, Pagliarani C, Savi T, Losso A, Cavalletto S, Tromba G, Dullin C, Bär A, Ganthaler A, Miotto A. 2018. The pitfalls of *in vivo* imaging techniques: evidence for cellular damage caused by synchrotron X-ray computed micro-tomography. New Phytologist **220**, 104–110.

Ponomarenko A, Vincent O, Pietriga A, Cochard H, Badel E, Marmottant P. 2014. Ultrasonic emissions reveal individual cavitation bubbles in water-stressed wood. Journal of the Royal Society Interface **11**, 20140480.

R Core Team. 2020. R: a language and environment for statistical computing. Vienna, Austria: R Foundation for Statistical Computing.

Rosner S, Karlsson B, Konnerth J, Hansmann C. 2009. Shrinkage processes in standard-size Norway spruce wood specimens with different vulnerability to cavitation. Tree Physiology **29**, 1419–1431.

Rosner S, Klein A, Wimmer R, Karlsson B. 2006. Extraction of features from ultrasound acoustic emissions: a tool to assess the hydraulic vulnerability of Norway spruce trunkwood? New Phytologist **171**, 105–116.

Sakes A, Van Wiel MD, Henselmans PWJ, Van Leeuwen JL, Dodou D, Breedveld P. 2016. Shooting mechanisms in nature: a systematic review. PLoS One **11**, 1–46.

Sperry JS, Donnelly JR, Tyree MT. 1988. A method for measuring hydraulic conductivity and embolism in xylem. Plant, Cell & Environment **11**, 35–40.

Tyree MT, Dixon MA. 1983. Cavitation events in *Thuja occidentalis* L.? Utrasonic acoustic emissions from the sapwood can be measured. Plant Physiology **72**, 1094–1099.

Tyree MT, Dixon MA, Thompson RG. 1984. Ultrasonic acoustic emissions from the sapwood of *Thuja occidentalis* measured inside a pressure bomb. Plant Physiology **74**, 1046–1049.

Tyree MT, Sperry JS. 1989. Vulnerability of xylem to cavitation and embolism. Annual Review of Plant Biology **40**, 19–36.

Urli M, Porté AJ, Cochard H, Guengant Y, Burlett R, Delzon S. 2013. Xylem embolism threshold for catastrophic hydraulic failure in angiosperm trees. Tree Physiology **33**, 672–683.

Vergeynst LL, Dierick M, Bogaerts JAN, Cnudde V, Steppe K. 2014. Cavitation: a blessing in disguise? New method to establish vulnerability curves and assess hydraulic capacitance of woody tissues. Tree Physiology **35**, 400–409.

Vergeynst LL, Sause MGR, De Baerdemaeker NJF, De Roo L, Steppe K. 2016. Clustering reveals cavitation-related acoustic emission signals from dehydrating branches. Tree Physiology **36**, 786–796.

Vergeynst LL, Sause MGR, Hamstad MA, Steppe K. 2015. Deciphering acoustic emission signals in drought stressed branches: the missing link between source and sensor. Frontiers in Plant Science **6**, 494.

Vilagrosa A, Morales F, Abadia A, Bellot J, Cochard H, Gil-Pelegrin E. 2010. Are symplast tolerance to intense drought conditions and xylem vulnerability to cavitation coordinated? An integrated analysis of photosynthetic, hydraulic and leaf level processes in two Mediterranean drought-resistant species. Environmental and Experimental Botany **69**, 233–242.

Wheeler JK, Huggett BA, Tofte AN, Rockwell FE, Holbrook NM. 2013. Cutting xylem under tension or supersaturated with gas can generate PLC and the appearance of rapid recovery from embolism. Plant, Cell & Environment **36**, 1938–1949.

Wolkerstorfer SV, Rosner S, Hietz P. 2012. An improved method and data analysis for ultrasound acoustic emissions and xylem vulnerability in conifer wood. Physiologia Plantarum **146**, 184–191.

Zweifel R, Item H, Häsler R. 2001. Link between diurnal stem radius changes and tree water relations. Tree Physiology **21**, 869–877.

Zweifel R, Zimmermann L, Newbery DM. 2005. Modeling tree water deficit from microclimate: an approach to quantifying drought stress. Tree Physiology **25**, 47–56.

Zweifel R, Zimmermann L, Zeugin F, Newbery DM. 2006. Intra-annual radial growth and water relations of trees: implications towards a growth mechanism. Journal of Experimental Botany **57**, 1445–1459.